NANO LETTERS

Letter

pubs.acs.org/NanoLett

Single Nanowire Photoconductive Terahertz Detectors

Kun Peng,[†] Patrick Parkinson,[‡] Lan Fu,[†] Qiang Gao,[†] Nian Jiang,[†] Ya-Nan Guo,[†] Fan Wang,[†] Hannah J. Joyce,[‡,§] Jessica L. Boland,[‡] Hark Hoe Tan,[†] Chennupati Jagadish,[†] and Michael B. Johnston*[,‡]

[†]Department of Electronic Materials Engineering, Research School of Physics and Engineering, The Australian National University, Canberra, ACT 0200, Australia

[‡]Department of Physics, University of Oxford, Clarendon Laboratory, Parks Road, Oxford, OX1 3PU, United Kingdom

[§]Department of Engineering, University of Cambridge, 9 JJ Thomson Avenue, Cambridge, CB3 0FA, United Kingdom

Supporting Information

ABSTRACT: Spectroscopy and imaging in the terahertz (THz) region of the electromagnetic spectrum has proven to provide important insights in fields as diverse as chemical analysis, materials characterization, security screening, and nondestructive testing. However, compact optoelectronics suited to the most powerful terahertz technique, time-domain spectroscopy, are lacking. Here, we implement single GaAs nanowires as microscopic coherent THz sensors and for the first time incorporated them into the pulsed time-domain technique. We also demonstrate the functionality of the single nanowire THz detector as a spectrometer by using it to measure the transmission spectrum of a 290 GHz low pass filter. Thus, nanowires are shown to be well suited for THz device applications and hold particular promise as near-field THz sensors.

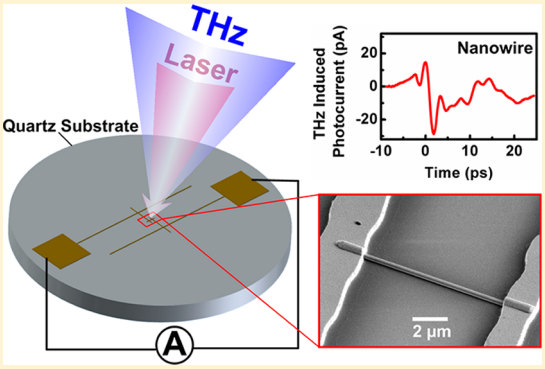

KEYWORDS: *Nanowire, terahertz optoelectronics, ultrafast, nano-optics*

Semiconductor nanowires based on III−V materials show great promise for nanoscale optoelectronic devices.[1−3] Such nanowires can be synthesized with diameters in the range of 10−500 nm and lengths of several micrometers, making them ideal for a variety of highly integrated applications. Recently a 13.8% efficient nanowire solar cell has been demonstrated,[4] while both GaAs-based[5,6] and InP-based[7] nanowires have been shown to operate as room-temperature nanolasers. Significantly, their high charge-carrier mobility[8] and tunable carrier lifetimes[9] make them ideal components for ultrafast electronics. Their application as terahertz (THz) frequency components is of particular interest owing to a lack of traditional electronic technologies in this wavelength range. Here, we demonstrate a photoconductive detector of THz frequency radiation that uses a single GaAs/AlGaAs nanowire as the active component. Our single nanowire THz detectors have good sensitivity when compared with traditional detection techniques including ion-implanted photoconductive antennae, but provide a novel opportunity to be used as highly integrated nanoscale devices.

Commercial THz systems typically use one of two techniques for THz detection: photoconductive (Auston) switches[10] using ion implantation-induced damaged[11] or low temperature grown[12] semiconductor materials; or optical rectification using electro-optical materials.[13] It is anticipated that III−V semiconductor nanowires may provide a promising alternative to planar semiconductor components in a THz system because they combine important bulk III−V semiconductor properties such as their direct and tunable band gap[14] and high carrier mobility,[8] with a short and controllable minority carrier lifetime, which is ideal for low noise photoconductive detection.[15] A nanowire-based detector also has great potential for near-field imaging either as a subwavelength detector element or integrated into an "on-chip" THz spectrometer[16] avoiding the need for complex coupling arrangements;[17−19] such devices are of interest for nanoscale[20] and biological[21] applications.

Nanowires have already been employed for THz spectroscopy as both emitting[22−24] or detecting elements. A bolometric InAs nanowire field-effect transistor detector has been demonstrated[25] and exploited for continuous-wave THz imaging applications.[26,27] More recently, a bolometric detector based upon carbon nanotubes has also been reported.[28] However, to date, such nanostructures have not been incorporated into the sensitive and widely applicable pulsed time-domain technique, partly due to challenges in material design, growth, and single nanowire device fabrication. We have previously shown that the minority carrier lifetime in GaAs-based nanowires can be tuned over the range of around 1 ps[9] to 1600 ps[29] through careful control of the crystal quality[30] and surface passivation.[29] It is now possible to design and grow GaAs nanowires, which couple short lifetimes with very high

Received: September 3, 2014
Revised: November 24, 2014
Published: December 9, 2014

   dx.doi.org/10.1021/nl5033843 | *Nano Lett.* 2015, 15, 206−210

carrier mobilities; these unique conductivity properties are optimal for the generation and detection of THz radiation directly through the photoconductive switch technique. Here we demonstrate the design, fabrication, and characterization of a single GaAs/AlGaAs nanowire photoconductive THz detector.

Three types of GaAs/AlGaAs core−shell nanowires were grown onto bulk GaAs substrates using a gold-assisted vapor−liquid−solid approach within a commercial MOCVD reactor. The growth methodology used followed previously published recipes;[29−32] more details are in the Supporting Information. These types of nanowires were chosen to investigate the effect of carrier lifetime upon detector performance. All nanowires had a GaAs/AlGaAs core−shell structure with a GaAs cap layer to prevent the oxidation of the AlGaAs shell, as shown in Figure 1. The first type, sample A, had a high-quality, monotypic zinc

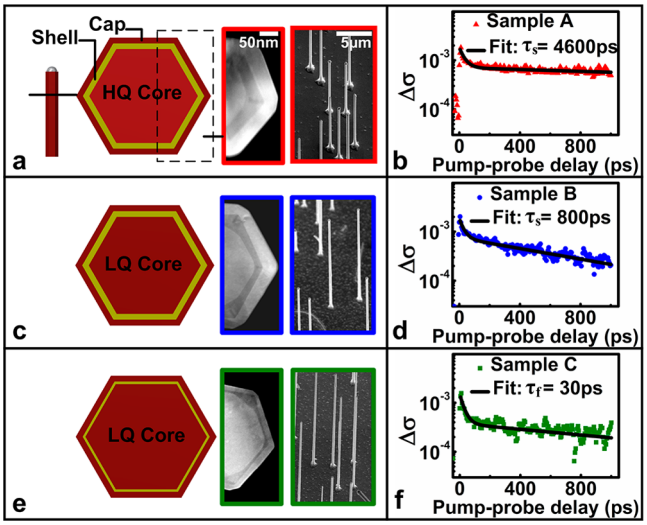

Figure 1. Schematics, electron micrograph images, and photoconductivity data of the nanowire samples. (Left) Schematic cross sections of the GaAs/AlGaAs core−shell nanowire used in this study. (Center) Typical cross-sectional TEM and SEM images of the three nanowire samples (the SEM images are taken with the surface tilted at 52° to the electron beam). (Right) Optical pump−THz probe photoconductivity. Solid black lines are a biexponential fit to the data. The labels show the dominant carrier lifetime for each sample.

blende stacking-fault-free GaAs core, grown by a two-temperature growth technique.[30] Both the second and third types, samples B and C, were intentionally grown to have a low-quality GaAs core incorporating stacking faults and defects known to reduce the carrier mobility and lifetime,[31] using a one-temperature growth technique. All nanowires have a 150 nm diameter core, an optimized AlGaAs shell[29] of 28 nm (samples A and B) or 5 nm (sample C) thickness, and were grown to mean lengths of around 13 μm (sample A) or 23 μm (samples B and C).

A time-domain optical pump−THz probe spectroscopy (OPTPS) system[8] was used to measure the conductivity lifetimes of an ensemble of nanowires from samples A, B, and C shown in Figure 1. Ultrafast photoexcitation at 800 nm (1.55 eV) was chosen to match the excitation conditions used under device operating conditions. The carrier lifetime is key to determining whether the detectors operate in the direct, integrating, or intermediate regime,[15] which in turn determines the signal processing technique required (see Supporting Information for details). We note that the ultimate temporal resolution of a photoconductive terahertz detector is set by the photoconductivity rise time and is much less than 1 ps for all samples shown for the excitation conditions described.[9] Traditional approaches to increasing the bandwidth of photoconductive detectors center around optimized damage of semiconducting material through ion-beam exposure[33] or low-temperature growth. A biexponential carrier lifetime was observed for all samples; a fast component (τ_f) due to recombination in the unpassivated GaAs capping layer and a slower recombination (τ_s) in the GaAs core, ranging from 4.6 ± 1 ns (sample A) to 800 ± 30 ps (sample B). Sample C exhibits a much larger early time carrier decay, arising from tunnelling through the thin AlGaAs shell layer to the highly defective capping layer in accord with our recent investigation into AlGaAs passivation.[29]

The THz detectors were fabricated using a custom-designed direct laser write lithography technique,[34] allowing electrical contacts to be made to single nanowires on THz transparent quartz substrates. Briefly, small pieces of substrate were cleaved from the as-grown wafers of samples A, B, and C, and placed in isopropyl alcohol (IPA) for a 30 s ultrasonication, to transfer the nanowires to solution. The solution was dropped onto z-cut quartz substrates and allowed to dry naturally. Z-cut quartz was used as detector substrates as it is an electrical insulator and transparent to THz radiation.[35] The THz detector structures were then patterned by use of direct laser write lithography.[34] After contact pattern development, an oxygen plasma etch was employed for further removal of the photoresist residue on the nanowires, followed by a 4% HCl chemical etch to remove a thin native oxide layer from the nanowire surface. The structures were finally metallized using electron beam evaporation and lift-off to form Ti/Au (10 nm/300 nm) contacts on each side of the nanowires.

The antenna structure and dimensions are shown in Figure 2a, along with a typical electron microscopy image of a complete device. Room-temperature photocurrent measurements were used to confirm the quality of the electrical contacts of the fabricated detectors (data in Supporting Information). With local excitation, such measurements can provide information about charge carrier mobility.[36] In our arrange-

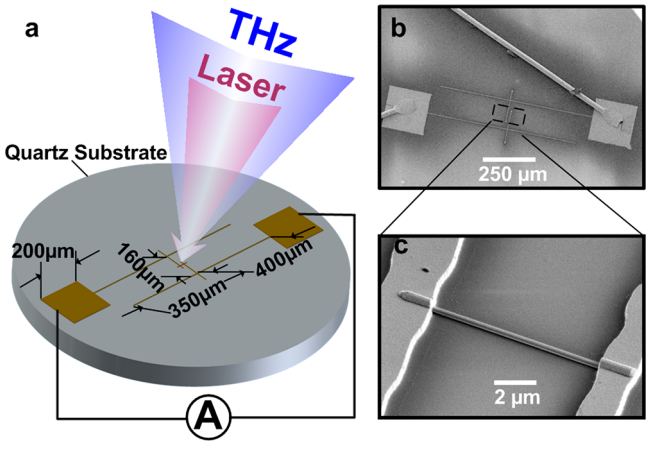

Figure 2. Detector design and micrograph of the fabricated devices (a) A schematic of the detector geometry (with dimensions) and optical arrangement used in this work. (b) A wide-area SEM image of a fabricated device. (c) A close up image of the central area of the device showing the nanowire.

dx.doi.org/10.1021/nl5033843 | Nano Lett. 2015, 15, 206−210

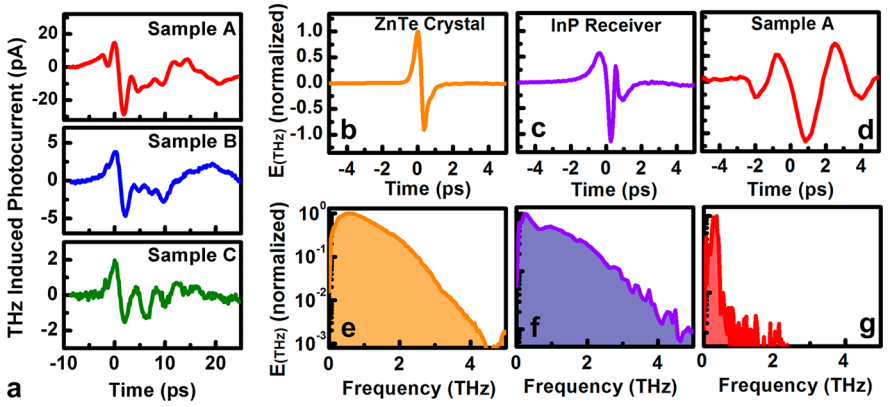

Figure 3. THz time-domain spectroscopy characterization of fabricated devices. (a) Unprocessed time-domain THz responses of the nanowire detectors measured in a THz-TDS system. (b–d) Processed and normalized THz electric field as measured by (b) a reference electro-optic sampling detector, (c) a reference InP photoconductive switch, and (d) sample A. (e–g) THz amplitude spectra corresponding to the electric field signals in panels b–d.

ment, we use uniform excitation, which provides photocurrent that is proportional to the carrier mobility; in turn, this determines the sensitivity of THz detection. All three samples show very low dark current (sub-nA) and a clear photoresponse under bias; sample A exhibits the strongest light response, with photocurrent exceeding 100 nA when biased at 4 V, confirming the improved electrical properties arising from the two-temperature growth technique. While sample B has the shortest charge-carrier lifetime, it is seen to exhibit a better photoresponse (10s of nA at 4 V) when compared with sample C (a few nA at 4 V).

The detectors were characterized using a THz time-domain spectrometer based around an 800 nm Ti:sapphire laser (THz-TDS, more details in the Supporting Information). A single cycle of THz radiation was generated using an AC-biased semi-insulating GaAs photoconductive switch with a 400 μm gap between the electrodes, which was focused onto a detector with a spot size of around 1 mm. A standard electro-optic detection crystal (ZnTe) was used as a reference detector to measure the electrical field of the THz source, while a photoconductive receiver[33] (ion-implanted InP with a bow-tie antenna structure) was used as a reference for our single nanowire devices. Figure 3a shows the typical unprocessed THz photocurrent responses of our single nanowire detectors measured in the THz-TDS system. All devices are integrating types[15] due to the long conductivity lifetimes in the core (≫100 ps) and produced pA responses with the detectors incorporating nanowires from samples A and C exhibiting the best and worst signal-to-noise ratio (SNR), respectively, which is consistent with results from DC photocurrent measurements (data in Supporting Information). All remaining measurements in this report focus on sample A, which forms the most sensitive detector. In addition, it is worth mentioning that the intensity of measured THz photocurrents from our nanowire detector increases with increasing intensity of the 800 nm pulse and/or the incident THz signal, but these do not influence the spectral profile.

The transient THz electric field as measured by the two reference detectors and the processed data for sample A, and their calculated spectral response are shown in Figure 3b–d and e–g, respectively (data and processing methods for all samples are given in the Supporting Information). While the signal measured using the nanowire has a lower bandwidth (in the range of 0.1–0.6 THz), it has sufficient SNR for practical use. To assess the performance of the nanowire detectors for real-world application we inserted a 290 GHz inductive mesh low-pass filter into the THz path, whose cutoff edge falls in the effective detection range of our nanowire detectors.

Figure 4 shows the THz responses from sample A and the InP photoconductive receiver, without (red) and with (blue)

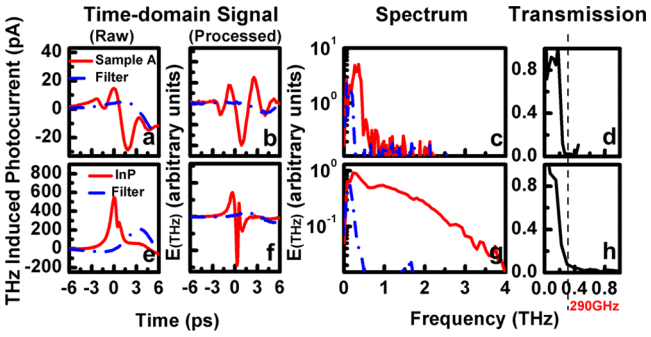

Figure 4. Comparative performance of (upper) nanowire-based and (lower) traditional detectors. (Left) Raw and processed time-domain THz electrical field. (Center) Amplitude spectrum of THz electrical field. (Right) Spectral change in amplitude and frequency due to the low-pass filter: (a–d) nanowire detector and (e–h) photoconductive InP receiver (red solid line, without filter; blue dash-and-dot line, with low-pass filter; black dashed line, cutoff frequency at 290 GHz).

the low-pass filter present. Figure 4d,h shows the filter transmission ratios, the changes of THz amplitude response in amplitude upon insertion of the low-pass filter. It can be clearly seen that both nanowire detector and reference InP detector show 80% transmission in amplitude due to the same filter. Therefore, single GaAs/AlGaAs nanowires are able to produce electrical responses to a THz signal, and when compared with standard THz detectors, such nanoscale devices bring many advantages for future applications whenever size or spatial resolution is critical, such as on-chip applications.[16,21]

Commercial software (Lumerical) based on the finite-difference time-domain (FDTD) method was used to perform simulations in the THz range to examine the influence of device geometry and compare with experimental results (details of the simulations are given in the Supporting Information). Figure 5a shows the experimental amplitude spectrum of the THz electrical field, while Figure 5b shows the simulated spectrum monitored at the center of the antenna. The introduction of the

dx.doi.org/10.1021/nl5033843 | Nano Lett. 2015, 15, 206–210

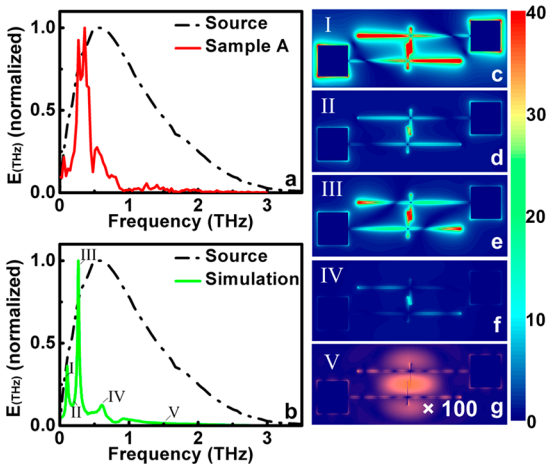

Figure 5. FDTD simulation of frequency response for the detector structure. (a) Experimentally determined amplitude spectrum of THz electrical field transient obtained using sample A. (b) FDTD simulated spectrum. (c–g) THz electrical field distribution at five different frequencies: I, 0.11 THz; II, 0.18 THz; III, 0.27 THz; IV, 0.61 THz; and V, 1.5 THz.

antenna structure alters the distribution of electric field, leading to enhancement at specific resonant frequencies. Figure 5c–g shows the THz electric field distribution on the antenna structure for five individual frequencies; it is clear that at frequency 'I' (0.11 THz), "III" (0.27 THz), and "IV" (0.61 THz) the THz electrical fields are strongly enhanced at the center of antenna, where the single nanowire is located. In contrast, there is very little field enhancement at the frequency "II" (0.18 THz) or 'V' (1.5 THz). It is worth noting that the experimental spectrum is consistent with the simulated spectrum, having similar bandwidth (0.1–0.6 THz) with three enhanced electric field peaks. This indicates that the detection bandwidth is caused by detector design, rather than the nanowire itself. In future, the use of a specific device geometry designed and optimized by modeling may be used to tune the frequency range and bandwidth of the detector.[37] The ability to tune the spectral response with nanoscale detectors is of promise for on-chip THz microspectrometers.[16,21]

In summary single GaAs/AlGaAs nanowire photoconductive THz detectors were successfully fabricated using a direct laser write lithographic technique and were shown to operate well over an effective detection range that may in future be adjusted through specific device geometries. FDTD simulation and experimental results were remarkably consistent; further work will focus on device geometry design and careful optimization of nanowire structure and growth. GaAs-based nanowires grown with specific and desirable carrier lifetime and carrier mobility provide great promise for highly integrated optoelectronics. By using careful growth control of the nanowire shell thickness and/or crystal quality, single nanowire photoconductive THz detectors have been fabricated. The demonstration of single GaAs/AlGaAs nanowire devices with a specific frequencies response through antenna design may lead to numerous potential applications for narrowband THz devices, for example, amplitude modulator/switches and tunable narrowband THz emitters or detectors.

■ ASSOCIATED CONTENT

Supporting Information

Details of nanowire growth, photocurrent measurements, electric field calculations, FDTD simulation, transmission electron microscopy, terahertz (THz) responses of single GaAs/AlGaAs nanowire detectors, THz-TDS system layout, and optical pump–terahertz probe photoconductivity measurements. This material is available free of charge via the Internet at http://pubs.acs.org.

■ AUTHOR INFORMATION

Corresponding Author

*E-mail: m.johnston@physics.ox.ac.uk.

Notes

The authors declare no competing financial interest.

■ ACKNOWLEDGMENTS

We acknowledge the Australian National Fabrication Facility (ANFF) ACT node for access to the fabrication facilities used in this work and the Engineering and Physical Sciences Research Council (EPSRC) for financial support. We thank Fouad Karouta (ANFF), Kaushal Vora (ANFF), Fang Fang Ren, Marco Zerbini, and Kam Chow (Lumerical Solution, Inc.) for useful discussions.

■ REFERENCES

(1) Duan, X. F.; Huang, Y.; Cui, Y.; Wang, J. F.; Lieber, C. M. *Nature* **2001**, *409*, 66–69.
(2) Li, Y.; Qian, F.; Xiang, J.; Lieber, C. M. *Mater. Today* **2006**, *9*, 18–27.
(3) Joyce, H. J.; Gao, Q.; Tan, H. H.; Jagadish, C.; Kim, Y.; Zou, J.; Smith, L. M.; Jackson, H. E.; Yarrison-Rice, J. M.; Parkinson, P.; Johnston, M. B. *Prog. Quantum Electron* **2011**, *35*, 23–75.
(4) Wallentin, J.; Anttu, N.; Asoli, D.; Huffman, M.; Aberg, I.; Magnusson, M. H.; Siefer, G.; Fuss-kailuweit, P.; Dimroth, F.; Witzigmann, B.; Xu, H. Q.; Samuelson, L.; Deppert, K.; Borgström, M. T. *Science* **2013**, *339*, 1057–1060.
(5) Saxena, D.; Mokkapati, S.; Parkinson, P.; Jiang, N.; Gao, Q.; Tan, H. H.; Jagadish, C. *Nat. Photonics* **2013**, *7*, 963–968.
(6) Mayer, B.; Rudolph, D.; Schnell, J.; Morkötter, S.; Winnerl, J.; Treu, J.; Müller, K.; Bracher, G.; Abstreiter, G.; Koblmüller, G.; Finley, J. J. *Nat. Commun.* **2013**, *4*, 2931.
(7) Gao, Q.; Saxena, D.; Wang, F.; Fu, L.; Mokkapati, S.; Guo, Y.; Li, L.; Wong-Leung, J.; Caroff, P.; Tan, H. H.; Jagadish, C. *Nano Lett.* **2014**, *14*, 5206–5211.
(8) Joyce, H. J.; Docherty, C. J.; Gao, Q.; Tan, H. H.; Jagadish, C.; Lloyd-Hughes, J.; Herz, L. M.; Johnston, M. B. *Nanotechnology* **2013**, *24*, 214006.
(9) Parkinson, P.; Lloyd-Hughes, J.; Gao, Q.; Tan, H. H.; Jagadish, C.; Johnston, M. B.; Herz, L. M. *Nano Lett.* **2007**, *7*, 2162–2165.
(10) Auston, D. H. *Appl. Phys. Lett.* **1975**, *26*, 101–103.
(11) Krotkus, A.; Marcinkevicius, S.; Jasinski, J.; Kaminska, M.; Tan, H. H.; Jagadish, C. *Appl. Phys. Lett.* **1995**, *66*, 3304–3306.
(12) Kono, S.; Tani, M.; Gu, P.; Sakai, K. *Appl. Phys. Lett.* **2000**, *77*, 4104–4106.
(13) Wu, Q.; Litz, M.; Zhang, X.-C. *Appl. Phys. Lett.* **1996**, *68*, 2924–2926.
(14) Wu, J.; Borg, B. M.; Jacobsson, D.; Dick, K. A.; Wernersson, L.-E. *J. Cryst. Growth* **2013**, *383*, 158–165.
(15) Castro-Camus, E.; Fu, L.; Lloyd-Hughes, J.; Tan, H. H.; Jagadish, C.; Johnston, M. B. *J. Appl. Phys.* **2008**, *104*, 053113.
(16) Cunningham, J.; Byrne, M. B.; Wood, C. D.; Dazhang, L. *Electron. Lett.* **2010**, *46*, S34–S37.
(17) Adam, A. J. L. *J. Infrared, Millimeter, Terahertz Waves* **2011**, *32*, 976–1019.

(18) Lecaque, R.; Grésillon, S.; Barbey, N.; Peretti, R.; Rivoal, J.-C.; Boccara, C. *Opt. Commun.* **2006**, *262*, 125−128.
(19) Hunsche, S.; Koch, M.; Brener, I.; Nuss, M. C. *Opt. Commun.* **1998**, *150*, 22−26.
(20) Cunningham, J.; Byrne, M.; Upadhya, P.; Lachab, M.; Linfield, E. H.; Davies, A. G. *Appl. Phys. Lett.* **2008**, *92*, 032903.
(21) Nagel, M.; Bolivar, P. H.; Brucherseifer, M.; Kurz, H.; Bosserhoff, A.; Büttner, R. *Appl. Phys. Lett.* **2002**, *80*, 154−156.
(22) Erhard, N.; Seifert, P.; Prechtel, L.; Hertenberger, S.; Karl, H.; Abstreiter, G.; Koblmüller, G.; Holleitner, A. W. *Ann. Phys.* **2013**, *525*, 180−188.
(23) Seletskiy, D. V.; Hasselbeck, M. P.; Cederberg, J. G.; Katzenmeyer, A.; Toimil-Molares, M. E.; Leonard, F.; Talin, A. A.; Sheik-Bahae, M. *Phys. Rev. B* **2011**, *84*, 115421.
(24) Arlauskas, A.; Treu, J.; Saller, K.; Beleckaitė, I.; Koblmüller, G.; Krotkus, A. *Nano Lett.* **2014**, *14*, 1508−1514.
(25) Vitiello, M. S.; Coquillat, D.; Viti, L.; Ercolani, D.; Teppe, F.; Pitanti, A.; Beltram, F.; Sorba, L.; Knap, W.; Tredicucci, A. *Nano Lett.* **2012**, *12*, 96−101.
(26) Romeo, L.; Coquillat, D.; Pea, M.; Ercolani, D.; Beltram, F.; Sorba, L.; Knap, W.; Tredicucci, A.; Vitiello, M. S. *Nanotechnology* **2013**, *24*, 214005.
(27) Ravaro, M.; Locatelli, M.; Viti, L.; Ercolani, D.; Consolino, L.; Bartalini, S.; Sorba, L.; Vitiello, M. S.; de Natale, P. D. *Appl. Phys. Lett.* **2014**, *104*, 083116.
(28) He, X.; Fujimura, N.; Lloyd, J. M.; Erickson, K. J.; Talin, A. A.; Zhang, Q.; Gao, W.; Jiang, Q.; Kawano, Y.; Hauge, R. H.; Léonard, F.; Kono, J. *Nano Lett.* **2014**, *14*, 3953−3958.
(29) Jiang, N.; Gao, Q.; Parkinson, P.; Wong-Leung, J.; Mokkapati, S.; Breuer, S.; Tan, H. H.; Zheng, C. L.; Etheridge, J.; Jagadish, C. *Nano Lett.* **2013**, *13*, 5135−5140.
(30) Joyce, H. J.; Gao, Q.; Tan, H. H.; Jagadish, C.; Kim, Y.; Zhang, X.; Guo, Y.; Zou, J. *Nano Lett.* **2007**, *7*, 921−926.
(31) Joyce, H. J.; Gao, Q.; Tan, H. H.; Jagadish, C.; Kim, Y.; Fickenscher, M. A.; Perera, S.; Hoang, T. B.; Smith, L. M.; Jackson, H. E.; Yarrison-Rice, J. M.; Zhang, X.; Zou, J. *Nano Lett.* **2009**, *9*, 695−701.
(32) Jiang, N.; Parkinson, P.; Gao, Q.; Breuer, S.; Tan, H. H.; Wong-Leung, J.; Jagadish, C. *Appl. Phys. Lett.* **2012**, *101*, 023111.
(33) Castro-Camus, E.; Lloyd-Hughes, J.; Fu, L.; Tan, H. H.; Jagadish, C.; Johnston, M. B. *Opt. Express* **2007**, *15*, 7047−7057.
(34) Parkinson, P.; Jiang, N.; Gao, Q.; Tan, H. H.; Jagadish, C. *Nanotechnology* **2012**, *23*, 335704.
(35) Grischkowsky, D.; Keiding, S.; van Exter, M.; Fattinger, C. H. *J. Opt. Soc. Am. B* **1990**, *7*, 2006−2015.
(36) Gu, Y.; Romankiewicz, J. P.; David, J. K.; Lensch, J. L.; Lauhon, L. J. *Nano Lett.* **2006**, *6*, 948−952.
(37) Janezic, M. D.; Baker-Jarvis, J. *IEEE Trans. Microwave Theory Tech.* **1999**, *47*, 2014−2020.